An *ab Initio* and Diffusion Monte Carlo Study of the Potential Energy Surface of the CO Dimer

Andrew W. Meredith[†]

Department of Physical Chemistry, The University of Göteborg, S-412 96, Göteborg, Sweden

Anthony J. Stone*

University Chemical Laboratory, Lensfield Road, Cambridge CB2 1EW, United Kingdom

Received: July 1, 1997; In Final Form: October 24, 1997[⊗]

A potential energy surface has been constructed for the CO dimer using the methods of intermolecular perturbation theory. The electrostatic and induction terms are described using distributed multipoles and distributed polarizabilities, the dispersion using anisotropic dispersion coefficients calculated by Rijks & Wormer, and the repulsion−penetration by an anisotropic exponential site-site function fitted to points calculated by *ab initio* intermolecular perturbation theory. The dispersion and induction are damped using Tang-Toennies damping functions. The potential has been used in diffusion Monte Carlo calculations of the ground rovibrational state, and the vibrationally averaged rotational constants agree well with experiment. The virial coefficient is also in good agreement with experiment. In order to achieve this agreement it is necessary to include C_9 and C_{10} dispersion terms. The potential energy surface has two symmetry-equivalent versions of each of two low-lying minima, both of which are planar and approximately T-shaped. A third minimum, with a planar, slipped anti-parallel structure, has also been located. There are two nonplanar paths between the lowest pair of minima, with a barrier of only about 30 cm^{-1}, and one planar path with a slightly higher barrier. In the lowest rovibrational state there is a high probability that the system is in the neighborhood of the barriers. Consequently, the vibrationally averaged rotational constants are significantly different from the values calculated for the equilibrium geometry.

I. Introduction

The CO dimer has recently been studied in a set of experiments by Havenith *et al.*[1] They observed a K_a:2 ← 1 subband of $(CO)_2$ and calculated, for the first time, some of the dimer's spectroscopic parameters. They interpreted the spectra as being consistent with a nonplanar structure for the dimer. This interpretation is apparently at odds with the the minima found on the *ab initio* surface of van der Pol *et al.*,[2] which were planar structures. That surface was found to be quite flat, with several planar minima separated by relatively small energy barriers.[2,3] Havenith *et al.* pointed to the possibility that the CO molecules execute wide angular oscillations in the vibrational ground state and that this might be responsible for the discrepancy between the interpretations of theory and experiment.

This suggests that further theoretical work is needed to try to understand the CO dimer and the nature of CO···CO interactions. In this study we derive a new *ab initio* potential energy surface for the CO dimer and perform diffusion Monte Carlo (DMC) and close-coupling calculations with this new surface in order to elucidate the lowest lying rovibrational states, the ground vibrational state, and vibrationally averaged properties.

The potential surface we derive is a refined surface based on that of van der Pol *et al.*, which was derived from the perturbation theory of intermolecular forces. This approach has the advantage that the interaction energy is separated quite naturally into terms which carry a clear physical interpretation—electrostatic, repulsion, dispersion, induction, and so on. The application of *ab initio* methods within a perturbative approach has been successful in rationalizing and predicting the structures and properties of Van der Waals complexes (see, for example, refs 4 and 5) and has led to new ideas and methods in formulating our description.[6−9] We draw upon some of these ideas in this study.

II. The Potential Energy Surface

1. Introduction. The new potential energy surface we have derived may be considered as a refinement of that of van der Pol *et al.* The differences between the new surface and that of van der Pol *et al.* is that induction effects are considered, the more recent calculations of the dispersion coefficients by Wormer[10] are included, a distributed multipole expansion is used to describe the electrostatic interactions, and the short range contributions to the potential energy surface are fitted using a multicenter description. In these calculations the CO bond length is held fixed at 1.128 Å.

2. Short-Range Terms. The first-order energy for the intermolecular interaction of two CO molecules was calculated by van der Pol *et al.*, at the SCF level, on a grid of intermolecular geometries.[2] This first-order energy can be partitioned, within perturbation theory, into an electrostatic term and a term describing the effects of exchange-repulsion.

* Corresponding author.

[†] Present address: Schlumberger Cambridge Research, High Cross, Madingley Road, Cambridge, CB3 0EL, U.K.

[⊗] Abstract published in *Advance ACS Abstracts,* December 15, 1997.

S1089-5639(97)02114-2 CCC: $15.00
Published on Web 01/08/1998

From their estimate of the first-order energy, we subtracted the multipolar approximation for the electrostatics, which we calculated using a three-site-distributed multipole analysis (DMA) obtained at the self-consistent field (SCF) level with the same basis, due to Schinke *et al.*,[11] that was used by van der Pol *et al.* This DMA was truncated at hexadecapole on each site and offers a more accurate evaluation of the electrostatic interaction since it implicitly includes the higher order terms beyond hexadecapole which would be needed in a single center expansion in order to obtain the same accuracy. On comparison with the overall moments of the molecule, the DMA expansion accurately reproduces all the SCF moments to hexadecapole (Q_4) and reproduces the 128-pole (Q_7) to within 15%. Using the same basis for the DMA as that of van der Pol's calculation of the first-order energy means that, after the subtraction of the multipolar energy, the remaining first-order energy is the sum of the exchange−repulsion energies and the SCF estimate of the penetration energy. As Wheatley and Mitchell have shown,[12] the penetration energy—the correction for the neglect of overlap effects in the multipolar expansion for the electrostatics—can be very significant, and its accurate calculation is important.

The partitioned sum of exchange-repulsion and penetration energies was fitted to an analytical site−site expression of the form

$$U_{\text{short}} = K \sum_a \sum_b \exp[-\alpha^{ab}(R_{ab} - \rho^{ab}(\Omega_{ab}))] \qquad (1)$$

Here K is a premultiplying factor of 1 mhartree, R_{ab} is the separation of sites a and b, and α^{ab} and ρ^{ab} are the site−site parameters describing the hardness and position of the repulsive walls, respectively.

The angular dependence of the site−site interactions was incorporated into the functional form by expanding the parameter ρ^{ab} as a series

$$\rho^{ab}(\Omega_{ab}) = \sum_{l_a l_b l} \rho^{ab}_{l_a l_b l} \bar{S}_{l_a l_b l}(\Omega_{ab}) \qquad (2)$$

The hardness parameter α^{ab} can in principle be anisotropic too, in which case it would be expanded in the same way, but we have not found it necessary to do so. That is, we need only the isotropic term α^{ab}_{000}. The functions $\bar{S}_{l_a l_b l}(\Omega)$ are members of the set of functions which form a complete basis for describing the dependence of any scalar property of a pair of sites, labeled a and b, on their relative orientation:[13,14]

$$\bar{S}_{l_a l_b l}(\Omega_{ab}) = \begin{pmatrix} l_a & l_b & l \\ 0 & 0 & 0 \end{pmatrix}^{-1} i^{l_a - l_b - l} \sum_{m_a, m_b, m} \begin{pmatrix} l_a & l_b & l \\ m_a & m_b & m \end{pmatrix} D^{l_a}_{m_a 0}(\omega_a) D^{l_b}_{m_b 0}(\omega_b) D^{l}_{m0}(\omega) \qquad (3)$$

$D^{l}_{m0}(\omega)$ is a Wigner rotation matrix;

$$\begin{pmatrix} l_a & l_b & l \\ 0 & 0 & 0 \end{pmatrix}$$

is a Wigner 3-j coefficient; ω_a, ω_b, and ω define the orientations of the molecules and the intersite vector in an arbitrary global axis system; and Ω_{ab} stands for the set of these orientations (ω_a, ω_b, ω). This formulation is completely general, and it can easily be used with a description in which the relative geometry is specified by a site−site distance R_{ab}, angles θ_a and θ_b describing the angles between the local site axes and the site−site vector, and a torsional angle φ_{ab}. (See Figure 1.)

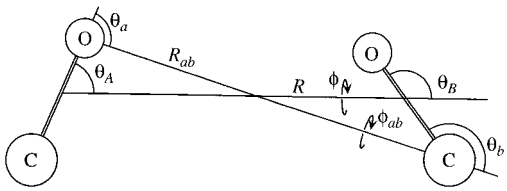

Figure 1. The coordinate system (R, θ_A, θ_B, φ) used to describe the geometry of the dimer, and the coordinates (R_{ab}, θ_a, θ_b, φ_{ab}) used to describe individual site−site interactions.

Although the $\bar{S}$ functions look quite complicated, the lower order functions are quite simple and are quick to evaluate. Those with $l_b = 0$ must have $l_a = l$, and they are the Legendre polynomials $P_l(\cos\theta_a)$, while those with $l_a = 0$ are the $P_l(\cos\theta_b)$. It is often quite a good approximation to use only $\bar{S}$ functions of this type, in which case eq 2 can be expressed in the form

$$\rho^{ab} = \rho^a(\theta_a) + \rho^b(\theta_b)$$

with

$$\rho^a(\theta_a) = \sum_l \rho^a_l P_l(\cos\theta_a), \quad \rho^b(\theta_b) = \sum_l \rho^b_l P_l(\cos\theta_b) \qquad (4)$$

The use of anisotropic potential forms need not mean that they cannot be used within simulations, as the work of Rodger *et al.*[15] has demonstrated. Many of the $\bar{S}$ functions and their derivatives are provided within the ORIENT program,[16] which can be easily interfaced with other programs.

The initial data of van der Pol *et al.* was on a grid of three values of R, five of φ, and six each of θ_A and θ_B. After the subtraction of the multipolar electrostatic term from the first-order energy, the remaining energies of the points on the grid had a distribution with a mean energy of 19.6 mhartree, a standard deviation of 40 mhartree, and a maximum energy of 315 mhartree. Since ambient temperature corresponds to an energy of 1 mhartree, it is apparent that quite a number of these points lie in regions which are thermally inaccessible. An accurate fit of the short-range data is important since the CO dimer has quite a flat potential surface, as previous calculations have indicated,[2,3] but the inclusion of the high-energy points makes it difficult to obtain a good fit in the thermally accessible region. Since we did not know *a priori* which geometries needed greater consideration, we retained all points with energy less than 10 mhartree. This truncation of the data set should mean that we comfortably span the region of the potential surface which is thermally accessible and emphasize the well region. Of the initial 315, a total of 199 points remained for use in the fitting procedure. The mean energy of these points was 2.82 mhartree, with a standard deviation of 2.80 mhartree. The distribution of geometries is no longer uniform, but the site−site distributions for the angular and radial sampling is still quite comprehensive, with most of the discarded points coming from geometries where the molecules were much closer than the van der Waals minimum.

The first model we tried was an isotropic site−site fit, using sites at C and O, but the results for this model were disappointing. The root mean square error for the difference between the *ab initio* values and the fitted surface was 0.6 mhartree, which is comparable with the estimated well depth of around 0.65

TABLE 1: Short-Range Coefficients Describing the Exchange−Repulsion and Penetration Contributions to the Interaction Energy for CO···CO[a]

component	C···C	O···C	O···O
Isotropic Model: Root Mean Square Error 0.600 mhartree			
α_{000}	2.5235	3.9384	5.0039
ρ_{000}	3.5401	3.0909	2.8502
Simple Anisotropic Model: Root Mean Square Error 0.078 mhartree			
α_{000}	3.0764	3.5349	3.8413
ρ_{000}	3.2215	3.1285	3.0581
ρ_{101}	−0.2032	−0.0595	−0.0557
ρ_{011}	−0.2032	−0.1907	−0.0557
Anisotropic Model: Root Mean Square Error 0.018 mhartree			
α_{000}	3.1569	3.5415	4.0477
ρ_{000}	3.3763	3.2387	2.9787
ρ_{101}	−0.0205	−0.1136	−0.1091
ρ_{011}	−0.0205	0.0804	−0.1091
ρ_{112}	0.0353	−0.0608	0.0876
ρ_{202}	0.1248	0.0556	0.0562
ρ_{022}	0.1248	0.2295	0.0562
ρ_{303}	0.0289	−0.0122	−0.0086
ρ_{033}	0.0289	0.0855	−0.0086
ρ_{123}	0.0030	−0.0692	−0.0209
ρ_{213}	0.0030	0.0170	−0.0209
ρ_{134}	−0.0100	−0.0343	−0.0054
ρ_{314}	−0.0100	−0.0071	−0.0054
ρ_{224}	0.0130	0.0105	0.0030

[a] The $\rho_{l_a l_b l}$ are expressed in Å, and α_{000} in Å^{-1}.

mhartree. Clearly the error in the isotropic fit is unacceptable, especially as the potential energy surface is expected to be quite flat.

The anisotropy of the site−site interactions can be described by adding terms in the angular expansion for the shape parameter ρ. The simplest of these models added the $\bar{S}_{101}$ and $\bar{S}_{011}$ terms (Table 1). These terms have a simple interpretation, amending the spherical shape of the repulsive wall of each site by adding a term which varies as $\cos(\theta)$. The standard deviation for this fit was 0.078 mhartree, a considerable improvement upon the isotropic model. The larger coefficients of this type are ρ_{101}^{CC}, ρ_{011}^{CC}, and ρ_{011}^{CC}, which are all about −0.2 Å. With our definition of the axis system, which has the positive sense of the body fixed z-axis going from C to O, the negative sign of ρ_{101}^{CC} indicates that the repulsive wall of the C atom is farther out when it is approached end on than when it is approached transversely. We can identify this with the larger spatial extent of the 5σ orbital on the C, which extends along the direction of the negative z-axis. Conversely, the negative value of about −0.05 Å for ρ_{101}^{OC}, ρ_{101}^{OO}, and ρ_{011}^{OO} shows that the repulsive wall of the O atom is farther out in the transverse direction than in the axial direction, which is consistent with the high π-electron density on the O atom, but the departure from spherical shape here is smaller. If eq 4 held exactly, then we would find that ρ_{011}^{CC} and ρ_{011}^{OC}would be equal, as would ρ_{101}^{OC} and ρ_{101}^{OO}. Table 1 shows that these relationships hold quite well, though not exactly.

Successive angular terms were added to improve the fit. Adding the terms ρ_{101}, ρ_{202}, and ρ_{303} reduced the standard deviation of the fit to 0.032 mhartree. Including all the angular functions that arise in the expansion of the electrostatic energy up to terms in R^{-5}, namely, those with $l_a + l_b = l$ and $l \leq 4$, reduced the standard deviation to 0.018 mhartree. The parameters for this fit are also given in Table 1. The geometrical interpretation in terms of the atomic shapes applies to some extent here too, but the additive picture of eq 4 does not apply when there are terms with l_a and l_b both nonzero.

TABLE 2: Distributed Multipole Moments for CO, in Atomic Units, Calculated at the MRCI-SD Level Using a [9s4p3d2f/9s5p3d2f] Basis[a]

site	Q_{00}	Q_{10}	Q_{20}	Q_{30}	Q_{40}
Two-Center Model					
C	0.0414	0.4242	−0.4221	0.7679	1.9499
O	−0.0414	−0.2632	0.3878	−0.8897	1.1583
Three-Center Model					
C	0.6038	1.0686	−0.2450	0.1172	0.1541
b	−0.9245	−0.2704	0.7506	−0.0416	0.3920
O	0.3207	−0.4235	0.1250	−0.1981	0.1278
Single-Site Model					
cm		0.0729	−1.52	3.61	−9.51
Experimental[17]					
cm		0.0432	−1.44		

[a] The site *b* is at the center of the bond. The positive *z*-axis is in the direction from C to O. The calculated and experimental[17] single-site moments are also given, relative to an origin at the center of mass (cm).

The isotropic coefficients α_{000} and ρ_{000} in all three models show that the C atom is more diffuse, having a greater spatial extent than the O atom. This is shown by the smaller value of α_{000} and the larger value of ρ_{000} for the C interactions when compared with those of O.

3. Electrostatics. It is now well established that a distributed description of the multipolar expansion is needed to describe electrostatic interactions in condensed phases to high accuracy.[7] In this study we have adopted such a description, using a three center DMA with expansion centers at the nuclear sites and at the bond center.

As is well-known, the dipole moment of CO is quite small.[17] This leads to problems with its *ab initio* calculation, and indeed the Hartree−Fock dipole moment for CO has the wrong sign. To reproduce the correct sign of the dipole in an *ab initio* calculation, which is desirable for the construction of an accurate CO dimer surface, it is necessary to use a correlated method. We have calculated the distributed multipoles of CO using a [9s4p3d2f/9s5p3d2f] basis at the MRCI-SD level. We constructed both two-center and three-center models, and the results are given in Table 2. For comparison between the DMA expansion and experiment we have calculated the overall moments. These are also shown in Table 2, and they show a slight overestimate of the dipole and quadrupole.

4. Dispersion. This term is particularly important when describing the interaction of weakly polar molecules, and we have used the MBPI estimates of the isotropic and anisotropic dispersion coefficients of Rijks and Wormer.[18]

The dispersion contributions to the energy are written as

$$U_{\text{disp}} = \sum_{n=6,7,\ldots} \sum_{l_a l_b l} f_n(\Omega;R)\, C_n^{l_a l_b l}\, \bar{S}_{l_a l_b l}(\Omega)$$

where f_n is a damping function, described below, $C_n^{l_a l_b l}$ are the dispersion coefficients, and $\bar{S}$ the set of angular functions described previously.

Since the initial calculations of Rijks and Wormer, a newer set of calculations have been made by them of the lower order dispersion coefficients:[10] C_6, C_7, and C_8. While both sets of calculations by Rijks and Wormer overestimate the anisotropy factors γ_{022} and γ_{224} for C_6 when compared with the experimental results of Kumar and Meath,[19] the overestimates for the newer set are significantly lower. For γ_{022}, the old values are

higher than experiment by 32%, compared with 14% for the newer set. Similarly for γ_{224} the old values are 75% higher, while the newer set are only 31% too high.

We have adopted the newer set of dispersion coefficients for our potential surface since they seem in better agreement with experiment. However because of restrictions in their basis set for their newer calculations, which went only as far as *f* functions, no estimates were made of the higher order dispersion coefficients C_9 and C_{10}. In our investigation of the potential energy surface, we have taken the coefficients for the C_9 and C_{10} interactions from the paper of van der Pol *et al.*,[2] and we consider the effects of their inclusion upon the potential energy surface.

Damping of the dispersion interactions is necessary at short range, but is perhaps one of the least-well-understood parts of the perturbation theory of intermolecular forces. Accurate calculations of overlap effects on dispersion and induction interactions have been carried out for a few atoms and for HF,[20] and several empirical functional forms have been developed to model these effects.[21] The most widely used of these are the damping functions of Tang and Toennies[22] which are given by the expression

$$f_n(b;R) = 1 - \exp(-bR)\sum_{k=0}^{n}\frac{(bR)^k}{k!}$$

where the parameter *b*, which is a measure of the overlap, is often identified with the repulsive parameter α. The damping function f_n multiplies the dispersion terms in R^{-n} and removes the divergence as the distance between the atoms tends to zero. For molecules with several atoms the damping should be anisotropic, and probably the argument of the damping function should be related to the logarithm of the repulsion energy, that is, to $\alpha(R - \rho(\Omega))$, rather than just to αR. However we have not explored this possibility, but have used isotropic damping functions with argument αR.

The values of the dispersion coefficients C_n are given in Table 3. The set of dispersion coefficients provided by Wormer,[10] as well as the C_9 and C_{10} coefficients taken from the paper of Rijks and Wormer,[18] contain more angular terms than shown in the table. We have removed a few of the high-order angular terms, whose coefficients were much less than 1% of the isotropic or first nonzero angular term. These terms were amongst the more exotic $\bar{S}$ functions. A test of the effect of their removal was made by calculating the second virial coefficient. They were found to have a negligible effect upon this property, suggesting that they are relatively unimportant.

5. Induction. We have included induction using the distributed polarizabilities calculated by Le Sueur.[23] In the distributed polarizability method[8] the response of a molecule to an applied field is partitioned amongst several sites. For CO these sites were at the nuclei. The distributed description of the polarizabilities takes account of the nonlocal response of the charge distribution, so that fields in one region of the molecule can lead to changes in the electron distribution at another. This leads to a distributed polarizability $\alpha'^{a,a}_{lk,l'k'}$, which describes how a field $V_{l'k'}$ (an *l*th derivative of the electrostatic potential) at site a' induces a moment ΔQ_{lk} at site *a*:

$$\Delta Q_{lk} = -\alpha^{a,a'}_{lk,l'k'}V_{l'k'}$$

The advantage of using a distributed description is that its convergence with respect to the rank of the polarizabilities is more rapid than for a single center expansion.[24]

TABLE 3: Dispersion Coefficients for the CO Dimer[a]

component	C_6	C_7	C_8	C_9	C_{10}
000	1845.0		20207.0		218274.6
101		−2739.7		−48948.0	
110			−1231.5		34134.4
112			3940.5		97522.4
202	197.2		13875.6		233997.2
211		61.2		7321.6	
213		−244.7		−21965.0	
220	4.4		182.9		15526.9
222	6.2		−382.5		−31151.1
224	67.2		2419.9		135925.6
303		77.9		−16197.0	
312			37.3		−8652.3
314			−165.5		27687.7
325		34.2		−994.3	
334			2.2		
336			76.6		−3670.7
404			−568.4		24771.3
415				1271.4	
422			−6.8		
424			−12.5		
426			−280.1		−3569.6
437				−441.6	
505				836.3	

[a] The C_6, C_7, and C_8 coefficients are taken from the more recent calculations of Wormer,[10] and the C_9 and C_{10} values are taken from the calculations of Rijks and Wormer.[2,18] The units of the C_n coefficients are given in mhartree Å^n. The origin for each molecule is at its center of mass. Because of symmetry constraints, $C_n^{l_a l_b l} = Cn^{l_b l_a l}$.

Induction damping. Damping must be applied to the induction energy for the same reasons as for the dispersion interactions. The induction energy involves site−site interactions; for molecule A in a dimer AB, it takes the form[14]

$$U_{\mathrm{ind}}^{\mathrm{A}} = -\frac{1}{2}\sum_{aa'bb'}\sum_{tt'uu'}(Q_u^b + \Delta Q_u^b)T_{ut}^{ba}\alpha_{tt'}^{aa'}T_{t'u'}^{a'b'}Q_{u'}^{b'} \qquad (5)$$

where *a* and a' are sites on molecule *A* and *b* and b' are sites on molecule B, while *t*, t', *u*, and u' are spherical tensor labels. $Q_{\boldsymbol{u}}^b$ is a static moment on site *b* of molecule B, and $\Delta Q_{\boldsymbol{u}}^b$ is the corresponding induced moment. In the case where $\alpha_{\boldsymbol{tt'}}^{aa'}$ is an ordinary dipole−dipole polarizability and $Q_{\boldsymbol{u}}^b$ is a component of the dipole moment, $T_{\boldsymbol{tu}}^{ab}$ and $T_{\boldsymbol{u't'}}^{b'a'}$ are dipole−dipole interaction tensors. If there is only one site on each molecule, then the overall interaction is proportional to R^{-6}, and because of the relationship between induction and dispersion the same damping function $f_n(b;R)$ is expected to apply. Where $a \neq a'$ or $b \neq b'$, however, we need to apply damping functions separately to $T_{\boldsymbol{tu}}^{ab}$, which depends on R_{ab}, and $T_{\boldsymbol{u't'}}^{b'a'}$, which depends on $R_{a'b'}$. It so happens that $[f_3(0.725b;R)]^2 \approx f_6(b;R)$; this approximation is quite good. We have therefore used damping factors of the form $f_3(0.725b;R)$ for each dipole−dipole interaction function $T_{\boldsymbol{tu}}^{ab}$, and in general $f_n(0.725b;R)$ for a multipole−multipole interaction function involving R^{-n}. The scale parameter *b* is taken to be equal to the hardness parameter α of the corresponding site−site repulsion.

It turns out that the effects of damping upon induction are not very significant around the van der Waals minimum, but when calculating the second virial coefficient and also in the DMC study, both of which sample the regions of space close to each molecule, the introduction of damping is necessary in order to avoid unphysical divergence of the induction at short range.

III. Development of the Potential Energy Surface

Initially we investigated a potential energy surface built from the best fit to the short-range data, the three-center DMA (MRCI-SD), the two-center DPA, and the C_6, C_7, and C_8 coefficients of Wormer.[10] Several minima and transition states were located on the surface, the lowest of which had an energy of −0.543 mhartree. We also calculated the second virial coefficient as a test of the potential's reliability. We found that this potential significantly underestimated $B(T)$ over the full range of temperatures that were measured experimentally. This would indicate that in a global sense the potential is not deep enough. This is borne out by the comparison of our estimate of −0.543 mhartree for the well depth, compared with −0.651 mhartree for the van der Pol *et al.* potential which gave excellent agreement with the experimental virial coefficients. This led us to consider the approximations behind our model.

One source of error lies with the use of SCF to estimate the first-order energy. Correlation certainly will have an effect upon the exchange−repulsion and penetration terms. However, experience has shown that this generally leads to a small increase in ρ, without significant changes in α. Any increase in ρ would enhance the repulsion and so lead to a shallower surface which will further increase the discrepancy with the experimental $B(T)$. Thus we discounted the omission of correlation effects from the first-order energy as being responsible for the disagreement with experiment. Similarly, we discounted basis set effects, since the first-order energy is not so sensitive to the quality of the basis, and even smaller double-ζ bases will recover much of the short range interaction. Errors from the fitting procedure are also unlikely to be the source of $B(T)$ discrepancy, since the standard deviation for the fit is only 0.018 mhartree.

The second possible source of error lies in the electrostatic description. The three-center DMA (MRCI-SD) is expected to be very good, although the dipole is still not reproduced exactly. Calculations were done with a single-center expansion, using the experimental multipole moments where available. This did not solve the discrepancy, and we ruled out the electrostatic description as being the source of the disagreement with experiment.

This led us to consider the induction terms. The distributed polarizabilities were calculated at the SCF level using a 5s4p2d basis. The restricted size of the basis, and the neglect of correlation, should be expected to underestimate the effects of induction. Comparing the SCF dipolar polarizability, calculated with the 5s4p2d basis, with the experimental dipolar polarizability, suggests that this error is of the order of 20%. However, the contribution of the induction energy to the calculated $B(T)$ at 77 K is only around -10 cm^3 mol^{-1}; while the experimental $B(T)$ is around -309 cm^3 mol^{-1} and induction adds only around 1.5% to the well depth at the minimum, it seems unlikely that induction accounts for the disagreement with experiment.

We conclude from all this that the model for the dispersion is the principal reason for the discrepancy with experiment.

IV. Analysis of the Dispersion Expansion

Apart from the work of Kumar and Meath[19] on the dipolar dispersion coefficients C_6, there are no other results with which we can judge the reliability of the MBPT dispersion coefficients of Wormer. The limited comparison which is possible suggests that the C_6 coefficients are reasonable, although they perhaps overestimate the anisotropy a little. However, there is currently no experimental method for probing the higher order dispersion coefficients, and we must accept the MBPT method as the best available source for these coefficients. The only parts of the dispersion model we can reasonably test in this study are the effects of damping, and whether our omission of the higher order C_9 and C_{10} terms can account for the discrepancy with the experimental $B(T)$.

1. Damping. The underestimate of $B(T)$, indicating that the potential energy surface is not deep enough, might indicate that we have overdamped the dispersion terms (C_6, C_7, and C_8). Certainly our model for the damping of the interaction is based on an empirical functional form. To explore the effect of damping we recalculated $B(T)$ after removing all damping terms. We found no significant improvement in the agreement with experiment and we conclude that errors in the damping model are not the cause of the discrepancy with experiment.

2. The Role of the Higher Dispersion Terms C_9 and C_{10}. We are left with the hypothesis that the discrepancy with the experimental $B(T)$ is due to the omission of the higher dispersion terms C_9 and C_{10}. The only estimates which have been published are those of Rijks and Wormer.[2,18] We have taken these coefficients and added them to our potential model, retaining the damping model we discussed earlier.

This extended potential surface was tested by calculating $B(T)$; as shown in the next section, the agreement with experiment was extremely good. This agreement was obtained without any scaling of the damping model for the dispersion terms, and although this is not conclusive, it would seem to support the functional form that we have used for the damping.

It would seem to indicate that the potential energy surface of the CO dimer is particularly sensitive to the effects of dispersion. The corollary of this is that any *ab initio* quantum chemistry study of the CO dimer should not only use correlated methods so as to include dispersion effects but also should use large basis sets in order to recover the dispersion energy accurately. The study of Woon on the Ar dimer[25] shows the slow convergence of the dispersion energy with basis set. A further point worth noting is that density functional studies using the current functionals, which are not able to describe the dispersion interaction properly, are unlikely to model the dimer accurately.

V. Evaluation of the Potential Energy Surface

The potential energy surface we have built consists of an anisotropic site−site model for the short-range interactions, a three-center DMA (MRCI-SD) for the electrostatics, a two-center DPA for the induction, and the dispersion coefficients of Rijks and Wormer up to terms in R^{-10} but with some of the smaller terms omitted. We have explored the topology of this surface and its spectroscopic properties both with and without the inclusion of induction. The induction energy is a relatively expensive term to calculate, and an estimation of its importance is relevant to the application of the model surface to extended systems.

In the following sections we explore the properties of the CO dimer on this potential energy surface by identifying its stationary points, calculating the second virial coefficients, performing close-coupling calculations to get the low-lying rovibrational states, and finally using the DMC method to calculate the spectroscopic constants of the dimer in its vibrational ground state.

VI. Topology of the Potential Energy Surface of the CO Dimer

The potential energy surface has been searched for its minima and transition states, using the ORIENT program.[16] This program uses eigenvector following methods to locate the

TABLE 4: Stationary Points on the CO Dimer Potential Surface Both with and without Induction

label	Hessian index	energy/cm^{-1}	geomety				frequencies/cm^{-1}			
			R/Å	θ_a	θ_b	φ				
			Induction Included							
M_1	0	−146.3	3.77	22.5	77.7	0	60.1	32.6	19.9	14.6
M_2	0	−118.1	4.41	94.9	0.9	0	58.1	34.4	21.0	8.9
M_3	0	−116.2	4.36	132.3	47.7	180	76.7	24.7	19.4	5.1
5_1	1	−114.8	3.51	76.9	103.1	19	45.6	31.7	5.7	25.0i
S_2	1	−110.9	3.90	37.8	142.2	180	46.1	23.7	11.0	13.3i
S_3	1	−116.6	4.27	77.8	25.5	0	52.7	36.6	18.4	11.2i
S_4	1	−116.0	4.39	120.6	34.3	180	73.8	26.5	19.3	6.0i
			No Induction							
M_1	0	−144.5	3.77	22.8	77.6	0	59.8	32.2	19.7	14.5
M_2	0	−113.7	4.43	96.8	2.2	180	58.6	32.8	19.6	6.1
M_3	0	−114.2	4.37	132.3	46.7	180	76.7	24.7	19.3	7.4
S_1	1	−113.6	3.51	76.7	103.3	19	45.5	31.2	5.8	24.6i
S_2	1	−110.2	3.91	38.0	142.0	180	44.1	23.8	10.9	11.4i
S_3	1	−113.0	4.32	74.6	23.2	0	50.7	36.3	17.9	11.2i
S_4	1	−113.4	4.43	111.4	22.5	180	68.5	28.5	19.0	6.1i

stationary points on the potential surface.[26] The first and second derivatives needed for the search are formed analytically. The results of the calculations for the potential energy surfaces both with and without induction are shown in Table 4. For comparison with the spectroscopic data presented later, we give the energies in cm^{-1}. The coordinate system we use to describe the dimer is shown in Figure 1.

We see that induction has relatively little effect upon the topology of the PES; the stationary points are virtually identical. The topology of the potential energy surface is seen to be quite interesting. We have located three minima and four transition states, all of them planar except for one of the transition states.

Both of the lowest lying minima can be loosely described as T-shaped complexes. The lowest of them, structure M_1, has the O end of one CO molecule pointing toward the other molecule, while the the other, M_2, has the C end of one molecule pointing toward the other molecule. These minima are separated by an energy difference of 30 cm^{-1}. Because each molecule can take the rôle of the head or the tail of the T, there are two versions of each of these minima, in the sense defined by Bone *et al.*;[27] that is, they differ only in the labeling of the identical nuclei.

The changeover between the C and O coordination in the T-shaped complexes as the radial separation is reduced from 4.4 to 3.8 Å suggests that this potential surface may be able to describe the head−tail disorder observed experimentally in the α phase of solid CO. In the $P2_13$-ordered phase of α CO,[28] the structure has a CO molecule pointing into a triangular arrangement of CO molecules, which are separated from this lone molecule by a distance of around 4 Å. At this separation the energy difference between the configurations with the O and C end respectively pointing at the molecules forming this triangle may be expected, on the basis of our calculations, to be quite small.

The harmonic frequencies at minimum M_1 suggest that the zero-point energy is around 64 cm^{-1}, which is over 40% of the calculated well depth. This would indicate that characterization of the stationary points alone may not allow one to infer the structure of the dimer, and it is possible that the secondary minima, labeled M_2 and M_3, may contribute to the vibrational ground state of the dimer. We expect the molecules to execute large amplitude motions, and Figure 2 shows that this zero-point energy is sufficient to allow not only large angular oscillations but also radial ones.

From an analysis of the stationary points, we find that S_1 is nonplanar (but nearly planar) C_2 saddle point linking the two versions of minimum M_1, S_2 is a planar C_{2h} saddle point linking the same minima M_1, S_3 is a C_s saddle point linking one of the versions of minimum M_1 with one of the versions of M_2, while S_4 is a C_s saddle point linking one of the versions of M_2 with M_3. According to the theorems derived by Bone *et al.*,[27] the number of symmetry-related versions of a stationary point is

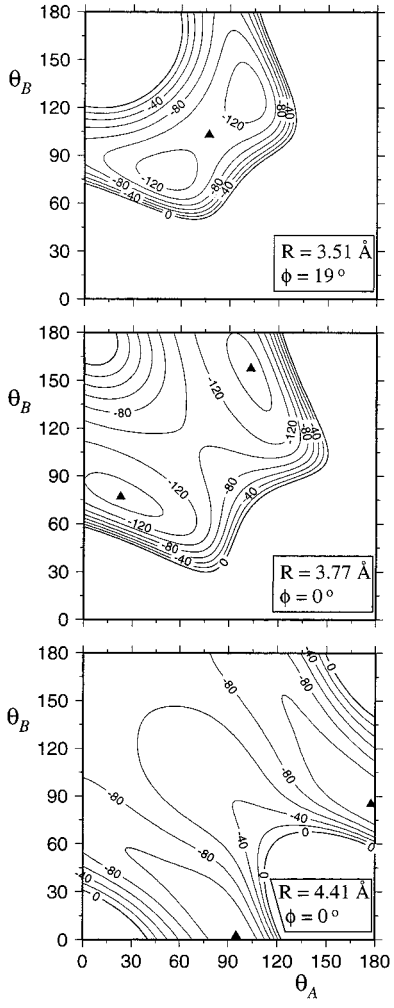

Figure 2. Contour plots of the interaction energy as a function of θ_A and θ_B around the stationary points S_1, M_1, and M_2. The radial separations and torsional angles are indicated in the figures. The contours are expressed in cm^{-1}, with a spacing of 20 cm^{-1} between adjacent contours. The stationary points from Table 4 are indicated by the filled triangles.

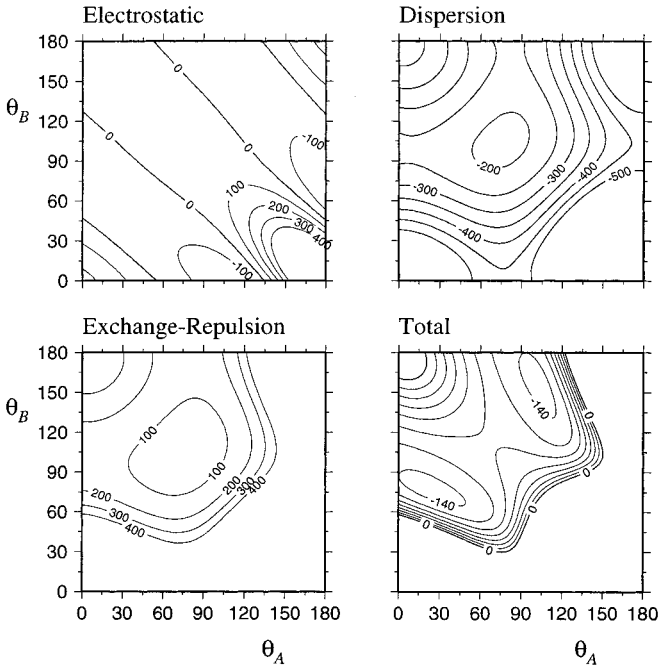

Figure 3. Contributions to the total interaction energy for planar geometries around the minimum M_1 ($\varphi = 0$, $R = 3.77$ Å). Contours are regularly spaced and are given in cm^{-1}.

equal to the order of the molecular symmetry group (4 for $(CO)_2$) divided by the order of the symmetry group of the stationary-point structure. Consequently there must be two versions of saddle points S_1, S_3, and S_4, but only one of S_2. The two versions of the S_1 saddle point are enantiomorphs of each other.

We have compared our potential with that of van der Pol *et al.* by recalculating the energy of the stationary points they identified. The surfaces compare reasonably well. The T-shaped structure which they calculated to have an energy of -140 cm^{-1} was calculated to have an energy of -137 cm^{-1} on our surface, and exact agreement was found for the planar structure with $r = 3.79$ Å, $\theta_A = 40°$, $\theta_B = 70°$, and $\varphi = 0°$. However, the agreement between the surfaces is not perfect, with one of the minima they identified, a slipped antiparallel structure with $r = 3.58$ Å, $\theta_A = 70°$, $\theta_B = 110°$, $\varphi = 180°$, having an energy of -139 cm^{-1} on their surface, but just -87 cm^{-1} on our surface. This is an important difference. The close-coupling calculations of Bunker *et al.*,[3] using the potential energy surface of van der Pol *et al.*, were interpreted on the basis that the tunneling motion between the symmetry related minima was *via* a C_{2h} (*i.e.*, a slipped antiparallel) transition state. The current surface does not favor this transition state geometry so heavily, and we may expect that the spectroscopy will differ. We return to this point later.

The advantage of perturbation theory is that it allows a physical insight into the nature of the interactions. In Figure 3 we plot the exchange−repulsion, electrostatic, and dispersion energies, as well as their total, for planar geometries ($\varphi = 0$) at $r = 3.79$ Å. This radial separation corresponds to that of the minimum M_1 and is close to the vibrationally averaged separation deduced experimentally.[1]

Examining Figure 3 we see that the total interaction is the result of a subtle balance between its various components. For planar configurations, electrostatics is seen to favor T-shaped orientations (which we attribute to the quadrupole) with a preference for the C end of one molecule to be coordinated with the other molecule. Since the molecular dipole is so weak, this preference in orientation must arise principally from the octopole. Dispersion is seen to favor C···C interactions, with the least favored planar geometry being when the molecules are both perpendicular to the intermolecular vector ($\theta_A \approx 90°$, $\theta_B \approx 90°$). Exchange−repulsion is seen to prefer these latter geometries, which minimize the interactions between the atomic sites, particularly the C···C interactions. This is related to the more diffuse nature of the C atom, and its associated lobe from the 5σ orbital. Together these figures go some way to explaining the topology of the potential energy surface. At larger separations the electrostatic interaction dominates, and we see a preference for T-shaped configurations with the C atom closest to the other molecule (minimum M_2), or a slipped antiparallel structure (minimum M_3). At short range exchange-repulsion dominates, and we see geometries which minimize the site−site interactions (transition state S_1). In the region of the van der Waals minimum we again see a T-shaped structure, but because of the greater repulsion associated with the C (relative to O), it is the O end which coordinates with the other molecule (minimum M_1).

Dispersion does make a substantial contribution, providing most of the binding energy. Indeed, at the separation corresponding to the minimum M_1, the sum of the electrostatic and exchange-repulsion energies is positive at all planar geometries. The topology of dispersion and exchange-repulsion contributions are seen to be complementary in the region of the van der Waals minimum M_1 (and also M_2) (*i.e.*, the most preferred geometry for the dispersion interaction is the least preferred for exchange−repulsion). At short-range, exchange−repulsion wins, and for this reason our discussion rationalizes the structure on the basis of electrostatics and exchange−repulsion. However, dispersion also favors minimum M_1 over M_2, because the smaller separation of the CO molecules when the O end is coordinated enhances the dispersion interaction.

Dispersion also contributes significantly to the anisotropy of the potential energy surface, and the differences between this potential surface and that of van der Pol *et al.* are partly attributable to the differences between the dispersion coefficients.

VII. Second Virial Coefficient

We have calculated the second virial coefficient $B(T)$ over the range of experimentally measured temperatures[29,30] using the potential energy surface. The classical contribution to $B(T)$ has been evaluated using the expression

$$B(T) = \frac{N_{av}}{4}\int_0^\infty\int_0^\pi\int_0^\pi\int_0^{2\pi}\left[1 - \exp\left(\frac{-U(R,\theta_A,\theta_B,\varphi)}{kT}\right)\right] R^2 \sin\theta_A \sin\theta_B \, dR \, d\theta_A \, d\theta_B \, d\varphi \quad (6)$$

Gaussian quadrature was used to integrate over the angles, while a Romberg method, based on the trapezoidal rule, was used to integrate over the radial coordinate. Integration over R was performed numerically between 2 and 30 Å, with the region of $R < 2$ Å approximated by the hard-sphere expression. The number of angular and radial points was increased until the results were stable. Quantum corrections to order $\hbar^2$, arising from the mean-squared force and torque, have been estimated by the Monte Carlo integration method programmed within ORIENT.

The results are given in Table 5. They show very good agreement with experiment, generally within the experimental error limits. A small increase (from 1.99 to 2.07) in the scale factor b used in the dispersion damping would bring all the

TABLE 5: Second Virial Coefficients, in cm³/mol, Calculated Using the Potential Energy Surface Described in the Text[a]

T (K)	B_{clas}	ΔB_q	B_{quant}	B_{exptl}	ΔB_{exptl}
77.3	−310.5	11.0	−299.5	−307.0	±5
90.1	−228.1	6.6	−221.5	−230.0	
143.0	−90.8	1.7	−89.1	−92.0	±4
173.0	−59.6	1.1	−58.5	−62.0	
213.0	−34.6	0.7	−33.9	−35.0	±3
242.0	−22.6	0.5	−22.1	−22.8	
263.0	−15.9	0.5	−15.4	−16.0	
273.0	−13.2	0.4	−12.8	−13.0	
298.1	−7.2	0.4	−6.8	−8.0	±2
323.3	−2.3	0.3	−2.0	−3.7	
348.2	1.7	0.3	2.0	1.1	
373.1	5.0	0.2	5.2	4.6	
398.1	7.9	0.2	8.1	7.7	
423.2	10.4	0.2	10.6	9.6	
473.2	14.5	0.2	14.7	14.5	±1
513.2	17.1	0.1	17.2	17.3	
573.2	20.1	0.1	20.2	20.5	

[a] In the final two columns the experimental values are shown,[29,30] together with the estimated experimental errors.

$B(T)$ values into agreement with experiment, within the experimental uncertainties.

VIII. Close-Coupling Calculations on the CO Dimer

The lowest lying rovibrational states have been calculated by a full close-coupling calculation using the program BOUND.[31] The CO bond lengths have been held fixed in these calculations, with a rotational constant of 1.9313 cm^{-1}. The numerical integration of the close-coupling equations used the diabatic logarithmic-derivative method, with a radial grid of 0.01 Å, integrating between 2 and 10 Å, with a matching point located at 4 Å. In choosing the rovibrational states that we calculate, we have restricted our calculations to those for which the total angular momentum J of the dimer is less than 2. This total angular momentum can be considered as being the result of coupling the angular momentum j_1 and j_2 of the molecules with that of the end-over-end angular momentum L of the complex, and thus we restrict ourselves to states where $j_1 + j_2 = L$. The number of channels included in the calculation (*i.e.*, the maximum j_1 and j_2 used in constructing the angular basis of primitive spherical harmonics) was increased until a reasonable degree of convergence was achieved.

The functional form used elsewhere in this paper is not immediately appropriate for the BOUND program since the analytic integrals used within that code depend upon the use of a single centre angular expansion. Accordingly we have translated our multicenter expansion to an expansion of the form

$$V(R,\theta_A,\theta_B,\varphi) = \sum_{l_a,l_b,l} \nu_{l_a,l_b,l}(R)\, g_{l_a,l_b,l}(\theta_A,\theta_B,\varphi) \qquad (7)$$

where the set of angular functions $g_{l_a,l_b,l}$ are related to the $\bar{S}_{l_a,l_b,l}$ functions by the relation

$$g_{l_a,l_b,l} = \frac{i^{l_a-l_b-l}(4\pi)^{3/2}(-1)^{l_a-l_b}}{\sqrt{(2l_a+1)(2l_b+1)}}\bar{S}_{l_a,l_b,l} \qquad (8)$$

The transformation to the single-center expansion was done on a grid of R values necessary for the evaluation of the bound state problem, with the angular coefficients $\nu_{l_a,l_b,l}(R)$ evaluated by numerical quadrature. In order to reproduce the multi-center expansions accurately it was necessary to use an expansion which went as far as $l_a = 8$, an expansion which has 285 coefficients (165 of which are unique). This expansion was sufficient to reproduce the potential to within 1% of the *ab initio* value in the region of the potential well.

TABLE 6: Calculated Eigenstates for $(CO)_2$, Expressed in cm^{-1}, for $J < 2$[a]

A^+		A^-	
$J = 0$	$J = 1$	$J = 0$	$J = 1$
22.4			
	20.5		
			20.1
			19.3
18.9			
	16.7		
	14.6		
		13.8	
			13.2
11.9			
			3.9
	2.4		
	2.1		
[−92.2]			

[a] These low-lying rovibrational states are calculated using a basis of primitive spherical harmonics, whose maximum angular momentum, j^{max}, was 6.

We performed the close-coupling calculations on the potential energy surface both with and without induction. The differences between these two sets of calculations were minimal: the energies of the lowest lying rovibrational states were practically the same, and the ordering of the states with respect to their symmetry and angular momentum were identical. The dissociation energy for the surface with induction was −93.6 cm^{-1}, while that for the surface without induction was −92.2 cm^{-1}. The results we display in Table 6 are for the potential surface which omits induction effects.

1. Results. The low-lying rovibrational states of the CO dimer are shown in Table 6. The states are labeled according to their angular momentum and symmetry. We use the molecular symmetry group[32,33] to provide the symmetry classification. Only rovibrational states of A symmetry are allowed for $(^{12}C^{16}O)_2$ because of nuclear spin statistics.

The dimer is seen to be quite weakly bound, with a dissociation energy of around 92 cm^{-1}. This is just one tenth of the value calculated for the HF dimer[34] and one quarter of that for the HCl dimer.[35]

While the selection rules $+ \leftrightarrow -$ and $\Delta J = 0, \pm 1$ are rigorous, the knowledge of the rovibrational states we have calculated does not give much information about the appearance of the dimer spectrum. An attempt was made to apply rovibrational labels to the eigenstates using the asymmetric top levels $J_{K_aK_c}$ and the normal modes of the dimer, following the approach taken by Bunker *et al.*[3] In the assignment of these labels, it is necessary to know the symmetries associated with the rotational and vibrational states, and for these the analysis of Hougen and Ohashi[36] was used, assuming that the tunneling motion occurred via the C_{2h} transition state.

For the different labeling schemes we devised within this scheme, we found contradictions in the relative ordering of states which we could not easily reconcile. Comparing our calculated rovibrational levels with those of Bunker *et al.* (which used the potential energy surface of van der Pol *et al.*) we see a qualitative difference in the relative ordering with respect to parity and angular momentum.

The failure to provide a spectral assignment in the same manner as Bunker *et al.* may reflect the role played in the

tunneling motion by the out of plane C_2 transition state, which will alter the splitting of the states. The C_2 and C_{2h} transition states (S_1 and S_2, respectively) are seen from Table 4 to be practically isoenergetic. The preferred tunneling path is explored in the next section on the DMC study.

The failure to provide a spectral assignment might be because the analysis of the rovibrational levels using the point group associated with the transition state is only valid in the high-barrier limit, and this combined with the expected anharmonicity of the upper levels, makes any assignment of the levels difficult using normal modes and asymmetric top labels.

Besides the spectral data of Havenith *et al.*, some spectral lines of the CO dimer were published by Vanden Bout *et al.*[37] The lines they found, which were assigned to the CO dimer on the basis of mass spectrometry, were used subsequently in an unsuccessful search for the CO dimer in the interstellar medium. The spectrum consisted of a single line at 0.05 cm^{-1}, and interestingly, a quartet of lines around 0.536 35 cm^{-1} with a separation of 0.000 019 cm^{-1}. The results from the close-coupling calculations do not provide any obvious agreement with these measurements. This might indicate an error in the potential surface, which we do not rule out. But an equally plausible explanation, based on the weak binding energy of the CO dimer, is that higher CO clusters are quite delicate and fragment quite easily. The observation by Vanden Bout *et al.* of a strong CO dimer peak in the mass spectrum, might reflect the fragmentation products of ionized CO clusters. Even the CO dimer complex is quite fragile, a property used by Havenith *et al.* in their concentration modulation of the dimer complex by an ac discharge. Further support for this argument comes from the quartet of lines, for which a simple explanation would be that we are observing the tunneling splittings arising from a cluster of 3 or more CO molecules. It is difficult to understand how a very small quartet splitting could arise in the CO dimer.

Without assignments of the levels, direct comparison with the experimental work of Havenith *et al.* is difficult. In the next section we use diffusion Monte Carlo to calculate the spectroscopic parameters of the CO dimer in its vibrational ground state and address the question of the preferred tunneling path.

IX. Diffusion Monte Carlo Study

1. Calculations. The ground state properties of the CO dimer have been calculated using the diffusion Monte Carlo method (DMC). In the light of our results showing that induction effects are relatively minor, we have performed these calculations on the surface without induction. This allows longer runs and so better statistics.

The DMC method,[38,39] which has been used to study electronic structure problems[40] and simulations of quantum solids, has been applied in recent years to the study of van der Waals complexes,[41] using the rigid body formulation of Buch.[42] A review of the DMC method has been given by Suhm and Watts.[39]

To calculate the spectroscopic constants averaged over the zero-point motion, and the ground state wave function, the method of descendent weighting was used.[38] All calculations for this paper were performed using QCLUSTER,[43] the DMC program of Sandler, which we interfaced with ORIENT.[16] We performed a series of seven runs over which the spectroscopic parameters, probability distributions, and zero-point energy of the dimer were calculated. Error limits were estimated from the standard deviations over the seven runs.

TABLE 7: Dissociation Energy and Vibrationally Averaged Rotational Constants for the CO Dimer in Its Ground State[a]

	this work	experimental[b]	Bunker *et al.*[c]
D_0	93.1(6)		94.7
A	1.59(2)	0.966	2.2
B	0.0785(4)		
C	0.0753(3)		
$^1/_2(B + C)$	0.0769(4)	0.0775	0.1
$(B - C)$	0.00321(9)	0.0002	

[a] The statistical uncertainty, estimated by the standard deviation between the different DMC runs, are given in brackets and refer to the last decimal place. All quantities are expressed in cm^{-1}. [b] Estimated for the ground state, $K = 1$, from the work of Havenith *et al.*[1] [c] Taken from the close-coupling calculations of Bunker *et al.*,[3] which used the potential of van der Pol *et al.*[2]

Each run involved the initial propagation of 1000 replicas over 7000 time steps to create a ground state distribution. The first 3000 of these steps were taken with a timestep of 30 au, which was decreased to 15 au for the remaining steps. After this equilibration, the descendent weighting method was used to calculate the probability distribution. The averaging was performed for nine generations of replicas simultaneously, with a delay of 100 steps between consecutive generations. Descendants were collected after an initial delay of 500 steps for 1000 steps.

2. Results. The DMC calculations confirm that, in its ground state, the CO dimer is practically a symmetric top ($B - C \simeq 0$), in agreement with the experiment of Havenith *et al.* The value that we calculate for $B - C$ is slightly larger than the experimental upper bound. This overestimate suggests that our model surface does not reproduce the more substantial out-of-plane motion indicated by the experiment. We should remember though that the rotational constant $B - C$ was measured for the state $K = 1$, and that our calculation is for the ground state $K = 0$. The extra angular momentum in $K = 1$ might be expected to lead to greater out-of-plane motion, more torsional averaging and a smaller $B - C$. However, we do not rule out the possibility that the overestimate of $B - C$ may be due to errors in our surface. High accuracy is needed for the accurate modeling of torsional motion, and small errors in the potential energy surface may have quite a large effect on this weakly bound system. It is possible in particular that the overestimate of $B - C$ is due to the omission of induction effects in these DMC calculations. It is encouraging that the agreement is so good, without any parameters being actively fitted for this *ab initio* potential surface.

The vibrationally averaged value for the rotational constant $^1/_2(B + C)$ shows excellent agreement with those measured experimentally. The experimental value we quote in Table 7 is for the state $K = 1$. When we consider that the experimental value for the state $K = 2$ is slightly larger than that for $K = 1$, we expect that the value that we calculate for the ground state (*i.e.* $K = 0$) should be just below the value for the $K = 1$ state, which indeed it is. The agreement between the estimates of the rotational constant A is not very good. However, it should be borne in mind that the estimate of Havenith *et al.* assumes that the complex is rigid and so does not allow for vibrational averaging effects.

The vibrationally averaged coordinates, shown in Table 8, cannot be compared easily with other calculations or experiments. The only figure that can be compared is the center of mass distance, and the agreement with the estimate of Havenith *et al.* reflects the accuracy with which the rotational constant

TABLE 8: Vibrationally Averaged Internal Coordinates of the CO Dimer in Its Ground State[a]

	this work	experimental[b]
R/Å	3.87(1)	3.86
θ_a	52(6)	
θ_b	114(7)	
φ	0(4)	

[a] The statistical uncertainty, estimated by the standard deviation between the different DMC runs, are given in brackets and refer to the last decimal place. Angles are in degrees. [b] Estimated for the ground state, $K = 1$, from the work of Havenith *et al.*[1]

$^1/_2\,(B + C)$ has been reproduced. The symmetry of the potential energy surface,

$$V(R,\theta_A,\theta_B,\varphi) = V(R,\pi - \theta_B,\pi - \theta_A,\varphi)$$

means that $\langle\theta_A\rangle = \pi - \langle\theta_B\rangle$. We see that this relation is almost true, within the estimated statistical errors of the DMC calculation.

Not surprisingly the average value of φ is zero, reflecting the fact that the DMC method samples all of the configurational space, and because the symmetry of the potential surface is such that $V(\varphi) = V(-\varphi)$, this assures an equal sampling of both positive and negative torsional configurations. The claims by Havenith *et al.* that the complex is nonplanar must be answered by a more careful appraisal of the torsional distribution and also by the feasibility of interchange between configurations on either side of the torsional plane on the timescale of the experiment.

The probability density ψ^2 projected onto the internal coordinates R, θ_A, and φ is shown in Figure 4. This figure shows that the CO dimer is a floppy complex which is undergoing large amplitude motions. The radial coordinate describing the intermolecular stretch has a distribution which extends over a range of 1.2 Å. Similarly the torsional coordinate φ, as well as the angular coordinate θ, show broad distributions.

Examining the φ distribution, we might characterize the complex as being a hindered rotor, and we should expect the torsional vibrational modes to be particularly anharmonic. The distribution is peaked around the planar configuration $\varphi = 0$. Considering this distribution, and the relatively small barriers to interconversion between the minima, we conclude that the CO dimer complex is planar on average, but it executes large amplitude motions in its torsional coordinate.

It is interesting to compare the CO dimer complex with the HF dimer. A DMC study of this latter complex[34] shows it to possess a similar floppiness. In this case the floppiness is probably related to the light mass of the hydrogens whereas for the CO dimer it is related to the shallowness of the potential energy surface (D_0 for the CO dimer is just one tenth of that for the HF dimer).

In the earlier section on the potential energy surface, we raised the possibility that the secondary minima (with the C end of one molecule pointing toward the second, or the slipped antiparallel structure) might contribute to the ground state. The range of the radial distribution does not preclude this. However, an examination of the distribution of θ_A shows that there is no significant probability for the C end of one molecule to point directly toward the other (the distribution dies off quite rapidly after $\theta_A = 120°$). The two peaks in the distribution are consistent with the complex adopting a structure dominated by the lowest minimum, and this is seen more clearly in the projection of ψ^2 onto θ_A and θ_B in Figure 5a. The positions of the minima and saddle points are shown on the same diagram.

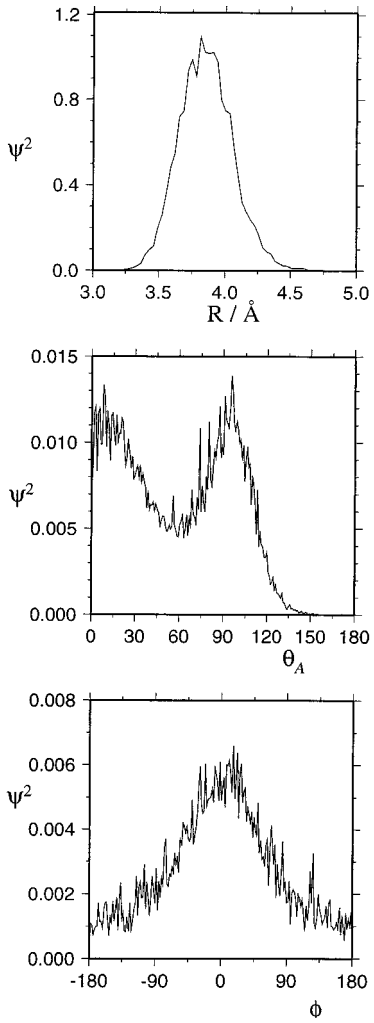

Figure 4. The normalized probability density for the CO dimer in its ground rovibrational state, projected onto the internal coordinates R, θ_A, and φ.

We also raised the question, in the earlier section on the close-coupling calculations, about the preferred tunneling motion between the minima. As is also seen in Figure 5b, a projection of ψ^2 onto the coordinate $\theta_s = \sqrt{1/_2}(\theta_A + \theta_B)$, there is a significant volume of space which links the symmetry related minima, and the CO dimer can be considered as being truly delocalized over the two potential wells. Interestingly, in the projection of ψ^2 onto the coordinates θ_A and θ_B, we see that the region of high ψ^2 linking the minima does not seem to correspond to the path over either type of saddle point. We must remember in this interpretation that Figure 5a is a projection onto θ_A and θ_B, so one path on this diagram could represent a multitude of different radial and torsional paths (subject to the constraint that the total angular momentum of the complex is conserved).

The reasons for the skewing of the probability distribution away from the saddle points can be seen from the zero-point energy. In the ground rovibrational state ($D_0 = 93$ cm^{-1}) the system lies above the potential energy associated with the transition states linking the minima. Furthermore, in the region of the transition states, the curvature of the potential energy surfaces is relatively gentle (the lowest frequencies associated with S_1 and S_2 are 6 and 11 cm^{-1}, respectively). This means that not only does the zero-point energy allow the system to pass over the barrier classically, but it may do so over a large region of space. The route by which the molecules in the

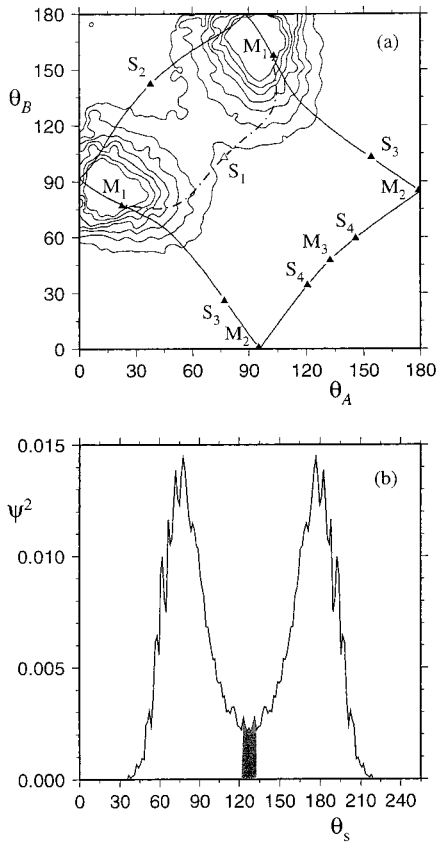

Figure 5. The normalized probability density for the CO dimer in its ground rovibrational state. (a) Projection of ψ^2 onto the (θ_A, θ_B) plane of the internal coordinates. Contours are drawn at intervals of 2.42×10^{-5}/degree^2, with the outer one representing a density of 2.42×10^{-5}/degree^2. The positions of the minima and saddle points are shown by the triangles, with filled triangles representing planar structures and the open triangle for S_1 denoting a nonplanar structure. The paths linking the stationary points are also shown, with solid lines indicating paths following planar geometries and the dot−dash line indicating a path through nonplanar geometries. (b) Projection of the probability density onto the axis of $\theta_s = \sqrt{1/2}(\theta_A + \theta_B)$ (the diagonal from bottom left to top right of the upper figure). The shaded area in the center shows the region which was sampled when examining the motion between the two wells (see Figure 6).

complex may pass between the symmetry related minima depends less on the exact position of the saddle point and more on the density of accessible configurations which link the minima.

Within a quantum mechanical view of transition state theory, the density of states associated with the transition state will guide the paths between the minima. S_1 (C_2 symmetry) has a low frequency mode of 6 cm^{-1} on our potential surface, compared with S_2 (C_{2h} symmetry), whose lowest frequency mode is 11 cm^{-1}. Thus the higher density of states associated with the low frequency mode of S_1 will favor a C_2 path. We should expect such a low-frequency mode to be very anharmonic, and this may well lead to a distribution whose center no longer coincides with the saddle point.

To confirm whether the C_2 path is the dominant one between the minima we have examined the probability density further. Because of the statistical noise associated with our DMC runs (we have 63 000 configurations distributed over the four dimensional space spanned by the internal coordinates) it is not possible to examine the gradients associated with the path between the minima. However, we can analyze the relative probability of configurations around the region of space linking the two wells.

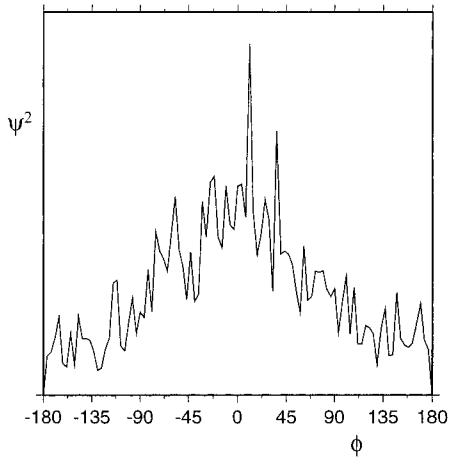

Figure 6. The unnormalized probability density for configurations of the CO dimer around the transition region between the two wells ($\theta_A = \pi - \theta_B$) projected onto the coordinate φ.

In Figure 6 we plot the φ distribution for configurations satisfying the condition $\theta_A = \pi - \theta_B \pm \delta\theta$. In this way we sample configurations linking the two wells. Choosing a value of 15° for $\delta\theta$ ensures that we sample a reasonable number of configurations to reduce the effects of statistical noise. Now, if the motion between the minima was dominated by the C_{2h} saddle point S_2, then allowing for a reasonable degree of torsional motion, we would expect the φ distribution of the sampled configurations to be concentrated around $\varphi = \pm\pi$, whereas if tunneling is via the C_2 saddle points S_1 we would expect the φ distribution to be concentrated in the region $-\pi/2 \leq \varphi \leq \pi/2$. Examining Figure 6, we conclude that motion between the minima is indeed dominated by C_2 configurations.

To further assess the validity of this conclusion, we examined the probability density around the C_{2h} and C_2 saddle points. Drawing a bounding volume around each saddle point, coordinates (R^S,θ_A^S,θ_B^S,φ^S), such that all replicas simultaneously satisfying the conditions:

$$|R^S - R| \leq R^{TOL}, \quad |\theta_A^S - \theta_A| \leq \theta^{TOL}, \quad |\theta_B^S - \theta_B| \leq \theta^{TOL}, \quad \text{and } |\varphi^S - \varphi| \leq \varphi^{TOL}$$

are considered as belonging to the transition state, we estimated their relative probabilities. Because of the statistical noise, we chose the following values of the tolerances: $R^{TOL} = 0.07$ Å, $\theta^{TOL} = 20°$, and $\varphi^{TOL} = 10°$. These are arbitrary values. They are chosen by trial and error to be large enough to reduce statistical errors from the sampling of the noisy DMC wave function, but small enough to be fairly local to the transition states. On this criterion, the system is 20 ± 6 times as likely to be in the neighborhood of one of the C_2 transition states than in the neighborhood of the C_{2h} one. This suggests strongly that the motion between the symmetry related minima is dominated by an out-of-plane C_2 geometry. These conclusions are in line with the out of plane tunneling suggested by Havenith *et al.* in their group theoretical analysis of the K_a:2 ← 1 subband of $(CO)_2$.

X. Conclusions

This study has led us to characterize the CO dimer as a planar but floppy T-shaped complex which undergoes large amplitude motions. It is practically a symmetric top in its ground state, as well as weakly bound, with a dissociation energy of around 93 cm^{-1}.

This study suggests that the CO dimer would be an interesting system for further study since it is an example of a floppy van der Waals complex, possessing a double well, with the barrier between the symmetry related minima being close to the zero-point energy associated with the intermolecular vibrations. There will be interference effects between the two equivalent C_2 tunneling paths, and it would be interesting to explore the sensitivity of the lowest rovibrational states to partial isotopic substitution, which would destroy the equivalence.

The tunneling path between the symmetry related minima is expected to be principally via an out-of-plane C_2 transition state, and so any group theoretical analysis of eigenstates of the dimer, along the lines of that of Hougen and Ohashi,[36] should be within a group containing the C_2 subgroup. The work of Havenith *et al.* used the C_2 point group to understand the spectrum, and the agreement between their work and the current one is encouraging. Apart from the development of a group theoretical understanding of the dimer, it would be interesting to see whether its rovibrational states can be simply understood using normal modes and symmetric top labels.

From the potential energy surface, constructed using perturbation theory, we characterize the complex as being bound principally through dispersion interactions. The structure of the complex is strongly influenced by the quadrupolar electrostatic interaction, favoring the T-shaped geometry, with the relative compactness of the O end of the molecule leading to coordination within the T-shaped complex *via* the O end of one molecule.

The agreement between the calculated virial coefficients and spectroscopic constants and the experimental values is quite good, and we believe that this potential energy surface provides a good representation for the dimer interaction. However, given the delicate balance of contributions to the overall interaction, a further study of the potential energy surface is necessary, and additional spectroscopic information would aid its refinement.

The importance of the higher order dispersion terms, and their influence upon the topology of the potential energy surface, makes this system diffficult for study with modern quantum chemistry methods—this system, if additional experimental measurements can be made, would be good for testing the limits of *ab initio* computation, particularly our representation of overlap effects (penetration and damping), for a weakly interacting molecular system.

The resolution of the effects of molecular symmetry on the spectrum has been studied in several van der Waals complexes. We believe that such effects will be resolvable in higher CO clusters (they may already have been observed by Vanden Bout *et al.*[37]), since CO···CO interactions are seen to be fairly weak, particularly induction, the principal three-body term, and so rearrangements of the CO molecules in clusters may be feasible on the time scale of some experiments.

Acknowledgment. We extend our thanks to Paul Wormer for kindly providing the raw *ab initio* data for the first-order energies from the work of van der Pol *et al.* and the revised set of dispersion coefficients. Pablo Sandler is thanked for making available his DMC program, QCLUSTER.

References and Notes

(1) Havenith, M.; Petri, M.; Lubina, C.; Hilpert, G.; Urban, W. *J. Mol. Spectrosc.* **1994**, *167*, 248.

(2) van der Pol, A.; van der Avoird, A.; Wormer, P. E. S. *J. Chem. Phys.* **1990**, *92*, 7498.

(3) Bunker, P.; Jensen, P.; Althorpe, S.; Clary, D. *J. Mol. Spectrosc.* **1993**, *157*, 208.

(4) Buckingham, A. D.; Fowler, P. W. *Can. J. Chem.* **1985**, *63*, 2018.

(5) Price, S. L.; Stone, A. J.; Lucas, J.; Rowland, R. S.; Thornley, A. *J. Am. Chem. Soc.* **1994**, *116*, 4910.

(6) Stone, A. J. *Chem. Phys. Lett.* **1981**, *83*, 233.

(7) Stone, A. J.; Price, S. L. *J. Phys. Chem.* **1988**, *92*, 3325.

(8) Stone, A. J. *Mol. Phys.* **1985**, *56*, 1065.

(9) Hayes, I. C.; Stone, A. J. *Mol. Phys.* **1984**, *53*, 83.

(10) Wormer, P. Personal Communication.

(11) Schinke, R.; Meyer, H.; Buck, U.; Diercksen, G. H. F. *J. Chem. Phys.* **1984**, *80*, 5519.

(12) Wheatley, R. J.; Mitchell, J. B. O. *J. Comput. Chem.* **1994**, *15*, 1187.

(13) Stone, A. J.; Tough, R. J. A. *Chem. Phys. Lett.* **1984**, *110*, 123.

(14) Stone, A. J. *The Theory of Intermolecular Forces*; International Series of Monographs in Chemistry; Clarendon Press: Oxford, 1996.

(15) Rodger, P.; Stone, A.; Tildesley, D. *Mol. Simul.* **1992**, *8*, 145.

(16) Stone, A. J.; Dullweber, A.; Popelier, P.; Wales, D. *ORIENT: a program for studying interactions between molecules*, version 3.2; University Chemical Laboratory; Cambridge, U.K., 1995.

(17) Meerts, W. L.; de Leeuw, F. H.; Dymanus, A. *Chem. Phys.* **1977**, *22*, 319.

(18) Rijks, W.; Wormer, P. E. S. *J. Chem. Phys.* **1989**, *90*, 6507.

(19) Kumar, A.; Meath, W. *Chem. Phys.* **1994**, *189*, 467.

(20) Knowles, P.; Meath, W. *Chem. Phys. Lett.* **1986**, *124*, 164. Knowles, P.; Meath, W. *Mol. Phys.* **1986**, *59*, 965. Knowles, P.; Meath, W. *Mol. Phys.* **1987**, *60*, 1143.

(21) Meath, W.; Koulis, M., *THEOCHEM. (J. Mol. Struct.)* **1991**, *72*, 1.

(22) Tang, K. T.; Toennies, J. P. *J. Chem. Phys.* **1984**, *80*, 3726.

(23) Le Sueur, C. R. Ph.D. thesis, University of Cambridge, 1991.

(24) Stone, A. J. *Chem. Phys. Lett.* **1989**, *155*, 111.

(25) Woon, D. *J. Chem. Phys.* **1994**, *100*, 2838.

(26) Wales, D. J. *Mol. Phys.* **1991**, *74*, 1. Wales, D. J. *J. Chem. Soc., Faraday Trans.* **1990**, *86*, 3505. Wales, D. J. *J. Chem. Soc., Faraday Trans.* **1992**, *88*, 653. Wales, D. J. *J. Chem. Soc., Faraday Trans.* **1993**, *89*, 1305.

(27) Bone, R. G. A.; Rowlands, T. W.; Handy, N. C.; Stone, A. J. *Mol. Phys.* **1991**, *72*, 33.

(28) Janssen, W. J. B. M.; Michiels, J.; van der Avoird, A. *J. Chem. Phys.* **1991**, *94*, 8402.

(29) Elias, E.; Hoang, N.; Sommer, J.; Schramm, B. *Ber. Bunsen-Ges. Phys. Chem.* **1986**, *90*, 342.

(30) Dymond, J.; Smith, E. *The Virial Coefficients of Pure Gases and Mixtures*; Oxford University; Oxford, 1980.

(31) Hutson, J. *BOUND* (computer code distributed via Collaborative Computational Project No. 6 on Heavy Particle Dynamics); UK Science and Engineering Research Council.

(32) Longuet-Higgins, H. C. *Mol. Phys.* **1963**, *6*, 445.

(33) Bunker, P. R. *Molecular Symmetry and Spectroscopy*; Academic Press: New York, 1979.

(34) Sun, H.; Watts, R. *J. Chem. Phys.* **1990**, *92*, 603.

(35) Elrod, M.; Saykally, R. *J. Chem. Phys.* **1995**, *103*, 933.

(36) Hougen, J.; Ohashi, N. *J. Mol. Spectrosc.* **1985**, *109*, 134.

(37) Vanden Bout, P.; Steed, J.; Berstein, S.; Klemperer, W. *Astrophys. J.* **1979**, *234*, 505.

(38) Kalos, M. *J. Comput. Phys.* **1967**, *2*, 1967.

(39) Suhm, M.; Watts, R. *Phys. Rep.* **1991**, *204*, 293.

(40) Anderson, J. *J. Chem. Phys.* **1975**, *63*, 1499. Anderson, J. *J. Chem. Phys.* **1976**, *65*, 4121. Anderson, J. *J. Chem. Phys.* **1980**, *73*, 3897.

(41) Sandler, P.; Jung, J. O.; Szczęśniak, M. M.; Buch, V. *J. Chem. Phys.* **1994**, *101*, 1378. Niyaz, P.; Bačić, Z.; Moskowitz, J.; Schmidt, K. *Chem. Phys. Lett.* **1996**, *252*, 23. Gregory, J.; Clary, D. *J. Chem. Phys.* **1995**, *102*, 7817.

(42) Buch, V. *J. Chem. Phys.* **1992**, *97*, 726.

(43) Sandler, P. *QCLUSTER: A quantum Monte Carlo simulation package.*